Progress In Electromagnetics Research B, Vol. 73, 79–93, 2017

The Development and Comparison of Two Polarimetric Calibration Techniques for Ground-Based Circularly Polarized Radar System

Yuta Izumi[1, *], Sevket Demirci[2], Mohd Z. Baharuddin[3], Mirza M. Waqar[1], and Josaphat T. Sri Sumantyo[1]

Abstract—Two techniques are described for the calibration of ground-based (GB) circularly polarized (CP) full polarimetric radars. The techniques are based on the point target calibration approach that uses various types of canonical reflectors with different orientations. Specifically, the calibration methods for linearly polarized (LP) radar proposed by Wiesbeck et al. and Gau et al. are selected and adapted to CP with suitable reflectors. The applicability of the techniques is examined through C-band scatterometric and synthetic aperture radar (SAR) measurements in an anechoic chamber. For the scatterometric mode, comparisons of calibrated channel imbalances with theoretical values show agreement within ± 0.3 dB in amplitude and $\pm 5^\circ$ in phase. The crosstalk between the channels is also reduced by ~ 5 to 30 dB after calibration. For the SAR mode, calibrated scattering matrix of a vertical wire target exhibits significant elimination of distortions between channel amplitudes and phases. The effect of calibration on target parameter retrieval is also investigated through the Cloud-Pottier eigenvector-based decomposition. Both calibration techniques are shown to yield improved accuracy of entropy-alpha (H-$\bar{\alpha}$) distributions and orientation angle ($\bar{\beta}$) values.

1. INTRODUCTION

Polarimetric synthetic aperture radar (Pol-SAR) has already known a powerful tool in quantitative remote sensing of Earth surface. Pol-SAR systems exploit polarimetric backscattering behavior of man-made and natural scatters for the derivation of bio- and geo-physical information of targets such as land, snow and ice, ocean, vegetation, and urban area [1–4]. In addition to its traditional use in airborne and spaceborne SAR systems, Pol-SAR is also increasingly used in various ground-based (GB) SAR applications such as vegetation monitoring, damage assessment of wooden building structure, and buried target detection [5–11].

Currently, most SAR systems employ linear polarization (LP), and various polarimetric processing techniques have been developed for LP-data. More recently, a SAR campaign in the Josaphat Microwave Remote Sensing Laboratory (JMRSL) of Chiba University in Japan has begun to use circularly polarized (CP) SAR [12–14] due to their advantages such as compactness, low power requirement and elimination of polarization mismatch losses caused by the Faraday rotation effect in the ionosphere [13, 15].

All multi polarimetric radars, however, should deal with challenging calibration problem which involves the removal of system-introduced polarimetric distortions such as polarimetric channel imbalances, crosstalk, and antenna gain. The scattering matrix contaminated by aforementioned distortions degrades the estimation of targets biophysical and geophysical parameters which is important for the Pol-SAR application. The calibration techniques reported in the literature can be categorized into two approaches namely; the natural target-based, and the point (or man-made) target-based

Received 6 January 2017, Accepted 8 March 2017, Scheduled 15 March 2017

* Corresponding author: Yuta Izumi (yutaizumi@chiba-u.jp).

[1] Center for Environmental Remote Sensing (CEReS), Chiba University, Japan. [2] Electrical and Electronic Faculty of Engineering, Mersin University, Turkey. [3] Department of Electronics and Communication Engineering, Tenaga National University, Malaysia.

techniques [16]. The first approach makes use of scattering properties of natural distributed targets to simplify the problem and is commonly used in airborne and spaceborne radars [17–20]. The second approach exploits known reflector targets and is best suited for high precision antenna measurements, radar cross section (RCS) measurements, and system validation through a GB radar. The latter case provides highly precise amplitude and phase information which is crucial to characterize the system's polarimetric capabilities truly.

To date, various point target-based calibration techniques have been developed for monostatic or quasi monostatic LP radars [21–27]. Yueh et al. generalized the concept using different combinations of three linearly independent calibration targets such as a wire, a dihedral, and a trihedral [21]. Sarabandi et al. developed a technique that requires only two calibration targets while assuming perfect isolation between horizontal (H) and vertical (V) polarization channels [22]. The technique proposed by Gau et al. also employs two point targets with simplification of the distortion matrix [23]. In addition, Whitt et al., Chen et al., and Wiesbeck et al. proposed a calibration technique without making any assumption about the distortion matrix by utilizing three reflector targets [24–27]. These well-developed point target-based calibration techniques have frequently been used for GB-SAR systems [5–11].

On the other hand, calibration of CP data is less studied since the vast majority of current radar systems that use LP. In [28], Michelson et al. introduced a modified algorithm for the point target-based CP calibration derived from the Chen et al.'s technique using a depolarizing trihedral corner reflector. However, this reflector is difficult to fabricate due to its complex structure [29, 30] and also no experimental results are given in this study. Hence, an investigation on the assessment of the calibration for CP systems is needed for upcoming CP-SAR missions.

In this study, two calibration approaches are proposed for calibrating the full-polarimetric GB CP radars. The LP-basis methods proposed by Wiesbeck et al. [26, 27] and Gau and Burnsid [23] are selected and adapted to CP because of their convenience for CP calibration. The performances of the derived techniques are assessed and compared through scatterometric and SAR imaging measurements inside an anechoic chamber.

The paper is organized as follows: the theory of the CP-basis calibration techniques is presented in the next section. Section 3 provides explanation of validation experiments and their results. Discussion of the results are given in Section 4. Last section concludes the paper.

2. POLARIMETRIC CALIBRATION METHODOLOGY FOR CP

In full polarimetric calibration, the contamination of the correct scattering matrix $[\mathbf{S^c}]$ is modeled by three distortion matrices: the receive error matrix $[\mathbf{R}]$, the transmit error matrix $[\mathbf{T}]$, and the isolation error matrix $[\mathbf{I}]$. The measured scattering matrix $[\mathbf{S^m}]$ can then be expressed as

$$[\mathbf{S^m}] = [\mathbf{R}]\,[\mathbf{S^c}]\,[\mathbf{T}] + [\mathbf{I}]\,, \tag{1a}$$

$$\begin{bmatrix} S_{11}^m & S_{12}^m \\ S_{21}^m & S_{22}^m \end{bmatrix} = \begin{bmatrix} R_{11} & R_{12} \\ R_{21} & R_{22} \end{bmatrix} \begin{bmatrix} S_{11}^c & S_{12}^c \\ S_{21}^c & S_{22}^c \end{bmatrix} \begin{bmatrix} T_{11} & T_{12} \\ T_{21} & T_{22} \end{bmatrix} + \begin{bmatrix} I_{11} & I_{12} \\ I_{21} & I_{22} \end{bmatrix}. \tag{1b}$$

For a GB radar, the isolation matrix $[\mathbf{I}]$ represents environmental noise such as reflection from undesired objects and coupling between transmitting and receiving antennas. Thus, it can be easily obtained by making a backscattering measurement without a target, called the empty room measurement [27]. To simplify the equation, the $[\mathbf{I}]$ can be replaced on the left side of (1a) and the empty room subtracted data $[\mathbf{M}]$ can be defined as:

$$[\mathbf{M}] = [\mathbf{S^m}] - [\mathbf{I}]\,. \tag{2}$$

With the knowledge of additive error matrix $[\mathbf{I}]$, the empty room calibrated model is described as:

$$[\mathbf{M}] = [\mathbf{R}]\,[\mathbf{S^c}]\,[\mathbf{T}]\,, \tag{3}$$

where it contains eight error coefficients to be determined. In point target-based calibration, the unknown coefficients in $[\mathbf{R}]$ and $[\mathbf{T}]$ are solved by the correct $[\mathbf{S^c}]$ and the measured $[\mathbf{M}]$ scattering matrices of several types of known canonical reflectors such as a sphere/circular plate, a vertical dihedral (i.e., at 0°), and a 45° inclined dihedral. For the calibration of our quasi-monostatic GB CP measurements, two techniques are proposed that deploy various combinations of the above-mentioned

calibration targets. Our approach is based on the adaptation of the LP based methods proposed by Wiesbeck et al. [26, 27] (hereafter denoted by CT1) and Gau and Burnsid [23] (hereafter denoted by CT2) to CP-basis. Throughout this paper, the proposed CP techniques derived from the CT1 and CT2 are named as CT1_CP and CT2_CP, respectively.

2.1. CT1_CP Calibration Process

Assuming empty room calibrated data, the CT1 solves the eight error coefficients of the complete polarimetric error model of (1b) by exploiting following reflectors with the order indicated below [27]:

$$\left[\mathbf{S^{c1}_{LP}}\right] = a\begin{bmatrix} 1 & 0 \\ 0 & 1 \end{bmatrix} \quad \text{(Sphere or Circular plate)}, \tag{4a}$$

$$\left[\mathbf{S^{c2}_{LP}}\right] = b\begin{bmatrix} -1 & 0 \\ 0 & 1 \end{bmatrix} \quad \text{(Vertical dihedral)}, \tag{4b}$$

$$\left[\mathbf{S^{c3}_{LP}}\right] = c\begin{bmatrix} 0 & 1 \\ 1 & 0 \end{bmatrix} \quad \text{(Dihedral 45°)}. \tag{4c}$$

where a, b, and c are complex constants related to target's RCS. Generally, all of these three linearly independent scattering matrices should be known to obtain the eight error coefficients.

For the adaptation of the CT1 to CP-basis, the calibration target types and/or their order should be changed accordingly. We propose herein the CT1_CP that incorporates a vertical dihedral as $[\mathbf{S^{c1}_{CP}}]$ and a dihedral 45° as $[\mathbf{S^{c2}_{CP}}]$ for the co-polarization calibration, and a circular plate as $[\mathbf{S^{c3}_{CP}}]$ for the cross-polarization calibration. A sphere can also be utilized instead of a circular plate but the circular plate has stronger response and thus easy identification. This choice is also suitable for quasi monostatic configuration [26].

It is well known that the scattering matrix in CP-basis can be linked to that in LP-basis via transformation [3]:

$$\begin{bmatrix} S_{LL} & S_{LR} \\ S_{RL} & S_{RR} \end{bmatrix} = \frac{1}{2}\begin{bmatrix} e^{j\theta} & 0 \\ 0 & e^{-j\theta} \end{bmatrix}\begin{bmatrix} 1 & j \\ j & 1 \end{bmatrix}\begin{bmatrix} S_{HH} & S_{HV} \\ S_{VH} & S_{VV} \end{bmatrix}\begin{bmatrix} 1 & j \\ j & 1 \end{bmatrix}\begin{bmatrix} e^{j\theta} & 0 \\ 0 & e^{-j\theta} \end{bmatrix}, \tag{5}$$

where j and θ indicate 90° phase shift and a line of sight orientation angle, respectively. Using Eq. (5), the true scattering matrices of the aforementioned reflectors can be obtained as:

$$\left[\mathbf{S^{c1}_{CP}}\right] = d\begin{bmatrix} -1 & 0 \\ 0 & 1 \end{bmatrix} \quad \text{(Vertical dihedral in CP basis)}, \tag{6a}$$

$$\left[\mathbf{S^{c2}_{CP}}\right] = e\begin{bmatrix} -e^{j90^\circ} & 0 \\ 0 & e^{-j90^\circ} \end{bmatrix} = e\begin{bmatrix} -j & 0 \\ 0 & -j \end{bmatrix} \quad \text{(Dihedral 45° in CP basis)}, \tag{6b}$$

$$\left[\mathbf{S^{c3}_{CP}}\right] = f\begin{bmatrix} 0 & j \\ j & 0 \end{bmatrix} \quad \text{(Sphere or Circular plate in CP basis)}. \tag{6c}$$

where d, e and f are RCS related to constants for CP backscattering. The negative sign in Eqs. (6a) and (6b) represents 180° phase shift.

The complete polarimetric error model in CP-basis has defined as:

$$\begin{bmatrix} S^m_{LL} & S^m_{LR} \\ S^m_{RL} & S^m_{RR} \end{bmatrix} = \begin{bmatrix} R_{LL} & R_{LR} \\ R_{RL} & R_{RR} \end{bmatrix}\begin{bmatrix} S^c_{LL} & S^c_{LR} \\ S^c_{RL} & S_{RR}{}^c \end{bmatrix}\begin{bmatrix} T_{LL} & T_{LR} \\ T_{RL} & T_{RR} \end{bmatrix} + \begin{bmatrix} I_{LL} & I_{LR} \\ I_{RL} & I_{RR} \end{bmatrix}, \tag{7}$$

where subscripts L and R represent left- and right-handed CP channels, respectively. As a first step in the derivation of the CT1_CP, the $[\mathbf{R}]$ and $[\mathbf{T}]$ matrices in Eq. (3) can be combined into a single error matrix $[\mathbf{E}]$ [26, 27]:

$$[\mathbf{M}] = [\mathbf{E}]\,[\mathbf{S^c}]\,, \tag{8}$$

which can be explicitly expressed as

$$\begin{bmatrix} M^i_{RR} \\ M^i_{LL} \\ M^i_{RL} \\ M^i_{LR} \end{bmatrix} = \begin{bmatrix} R_{RR}T_{RR} & R_{RL}T_{LR} & R_{RR}T_{LR} & R_{RL}T_{RR} \\ R_{LR}T_{RL} & R_{LL}T_{LL} & R_{LR}T_{LL} & R_{LL}T_{RL} \\ R_{RR}T_{RL} & R_{RL}T_{LL} & R_{RR}T_{LL} & R_{RL}T_{RL} \\ R_{LR}T_{RR} & R_{LL}T_{LR} & R_{LR}T_{LR} & R_{LL}T_{RR} \end{bmatrix} \begin{bmatrix} S^{ci}_{RR} \\ S^{ci}_{LL} \\ S^{ci}_{RL} \\ S^{ci}_{LR} \end{bmatrix}$$
$$= \begin{bmatrix} \varepsilon_{11} & \varepsilon_{12} & \varepsilon_{13} & \varepsilon_{14} \\ \varepsilon_{21} & \varepsilon_{22} & \varepsilon_{23} & \varepsilon_{24} \\ \varepsilon_{31} & \varepsilon_{32} & \varepsilon_{33} & \varepsilon_{34} \\ \varepsilon_{41} & \varepsilon_{42} & \varepsilon_{43} & \varepsilon_{44} \end{bmatrix} \begin{bmatrix} S^{ci}_{RR} \\ S^{ci}_{LL} \\ S^{ci}_{RL} \\ S^{ci}_{LR} \end{bmatrix}. \tag{9}$$

The sixteen error coefficients of $[\mathbf{E}]$ can be reduced to eight by sequential substitution as

$$\begin{bmatrix} M^i_{RR} \\ M^i_{LL} \\ M^i_{RL} \\ M^i_{LR} \end{bmatrix} = \begin{bmatrix} \varepsilon_{11} & \dfrac{\varepsilon_{32}\varepsilon_{42}}{\varepsilon_{22}} & \dfrac{\varepsilon_{33}\varepsilon_{42}}{\varepsilon_{22}} & \dfrac{\varepsilon_{32}\varepsilon_{11}}{\varepsilon_{33}} \\ \dfrac{\varepsilon_{31}\varepsilon_{41}}{\varepsilon_{11}} & \varepsilon_{22} & \dfrac{\varepsilon_{33}\varepsilon_{41}}{\varepsilon_{11}} & \dfrac{\varepsilon_{31}\varepsilon_{22}}{\varepsilon_{33}} \\ \varepsilon_{31} & \varepsilon_{32} & \varepsilon_{33} & \dfrac{\varepsilon_{32}\varepsilon_{31}}{\varepsilon_{33}} \\ \varepsilon_{41} & \varepsilon_{42} & \dfrac{\varepsilon_{42}\varepsilon_{41}}{\varepsilon_{44}} & \varepsilon_{44} \end{bmatrix} \begin{bmatrix} S^{ci}_{RR} \\ S^{ci}_{LL} \\ S^{ci}_{RL} \\ S^{ci}_{LR} \end{bmatrix}. \tag{10}$$

Theoretically, these eight unknowns can be determined through measurements of at least two calibration targets that produce four linearly independent backscattering coefficients. However, due to difficulty in finding such a target set, three calibration targets were selected in the CT1_CP with known scattering matrices $[\mathbf{S}^{ci}]$ where $i = 1$, 2, and 3 represent a vertical dihedral, dihedral 45°, and circular plate, respectively. Invoking the reciprocity condition ($S_{LR} = S_{RL}$), the error coefficients are computed by the following equations:

$$\varepsilon_{11} = \frac{S^{c2}_{LL}M^1_{RR} - S^{c1}_{LL}M^2_{RR}}{\left(S^{c1}_{RR}S^{c2}_{LL} - S^{c1}_{LL}S^{c2}_{RR}\right)}, \tag{11}$$

$$\varepsilon_{22} = \frac{S^{c1}_{RR}M^2_{LL} - S^{c2}_{RR}M^1_{LL}}{\left(S^{c1}_{RR}S^{c2}_{LL} - S^{c1}_{LL}S^{c2}_{RR}\right)}, \tag{12}$$

$$\varepsilon_{31} = \frac{S^{c2}_{LL}M^1_{RL} - S^{c1}_{LL}M^2_{RL}}{\left(S^{c1}_{RR}S^{c2}_{LL} - S^{c1}_{LL}S^{c2}_{RR}\right)}, \tag{13}$$

$$\varepsilon_{33} = \frac{M^3_{RL}}{2S^{c3}_{RL}} \pm \sqrt{\left(\frac{M^3_{RL}}{2S^{c3}_{RL}}\right)^2 - \varepsilon_{31}\varepsilon_{32}}, \tag{14}$$

$$\varepsilon_{32} = \frac{S^{c1}_{RR}M^2_{RL} - S^{c2}_{RR}M^1_{RL}}{\left(S^{c1}_{RR}S^{c2}_{LL} - S^{c1}_{LL}S^{c2}_{RR}\right)}, \tag{15}$$

$$\varepsilon_{41} = \frac{S^{c2}_{LL}M^1_{LR} - S^{c1}_{LL}M^2_{LR}}{\left(S^{c1}_{RR}S^{c2}_{LL} - S^{c1}_{LL}S^{c2}_{RR}\right)}, \tag{16}$$

$$\varepsilon_{42} = \frac{S^{c1}_{RR}M^2_{LR} - S^{c2}_{RR}M^1_{LR}}{\left(S^{c1}_{RR}S^{c2}_{LL} - S^{c1}_{LL}S^{c2}_{RR}\right)}, \tag{17}$$

$$\varepsilon_{44} = \frac{M^3_{LR}}{2S^{c3}_{RL}} \pm \sqrt{\left(\frac{M^3_{LR}}{2S^{c3}_{RL}}\right)^2 - \varepsilon_{41}\varepsilon_{42}}. \tag{18}$$

It should be noted that the sign of the error coefficients given in Eq. (14) can be determined by dominating diagonal elements given in Eq. (9) as $|\varepsilon_{33}| \gg |\varepsilon_{34}|$ and the condition of $\angle(\varepsilon_{33} + \varepsilon_{34}) \approx \angle\varepsilon_{33}$. The sign of the term in Eq. (18) can be selected in a similar manner.

After all error coefficients are determined, calibrated CP-radar data $[\mathbf{S^c}]$ is solved by inversion of Eq. (8), given as below:

$$[\mathbf{S^c}] = [\mathbf{E}]^{-1}[\mathbf{M}]. \tag{19}$$

The CT1 and the proposed CT1_CP require the knowledge of the theoretical $[\mathbf{S^{c3}}]$ of a circular plate, $[\mathbf{S^{c1}}]$ of a vertical dihedral, and $[\mathbf{S^{c2}}]$ of a dihedral 45°. It is occasionally difficult to exactly compute the scattering matrices of a dihedral and an inclined of dihedral which are regarded as complex targets. These factors can lead to errors between the theoretical and actual values of the scattering matrices which may degrade the accuracy. Nevertheless, this problem can be mitigated if an approach similar to the single reference calibration technique proposed by Wiesbeck and Kahny [26] can be exploited. In this LP-basis technique, the knowledge of theoretical scattering matrix is required for only one reference target such as a circular plate or a sphere. These targets are easy to align and their scattering matrices can be calculated very precisely [31]. The correct scattering matrices of other complex dihedral targets are derived from this reference target's data. Briefly, the technique makes use of similar forms of the scattering matrices from a simple (sphere or circular plate) and a complex target (dihedral) to calculate the correct matrix of the latter one. Unfortunately, this methodology cannot be directly applicable to CP-basis, since there is no such a pair of calibration targets (see (6)). The literature which we previously demonstrated a polarimetric calibration for GB CP-SAR without single reference calibration concept produced improved results of RCS and amplitude and phase imbalance but significant residual errors are still remained [32]. One possible solution might be to conduct the single reference calibration on LP-basis by transforming from CP to LP basis. The flowchart of this proposed single reference calibration technique adopted in CT1_CP is explained in Fig. 1. In this approach, the correct scattering matrix of a vertical dihedral is first calculated in LP-basis by known reference target's data (i.e., $\mathbf{S^{c3}}$ and $\mathbf{M^3}$ of circular plate) and its measurement data (i.e., $\mathbf{M^1}$) with the following equation

$$\begin{bmatrix} S^{c1}_{HH} \\ S^{c1}_{VV} \end{bmatrix} = \begin{bmatrix} \dfrac{S^{c3}_{HH}}{M^3_{HH}} & 0 \\ 0 & \dfrac{S^{c3}_{VV}}{M^3_{VV}} \end{bmatrix} \begin{bmatrix} M^1_{HH} \\ M^1_{VV} \end{bmatrix}, \tag{20}$$

wherein the cross-polarization components are assumed to be negligible. The obtained partially theoretical scattering matrix of the vertical dihedral is then transformed from LP to CP basis using

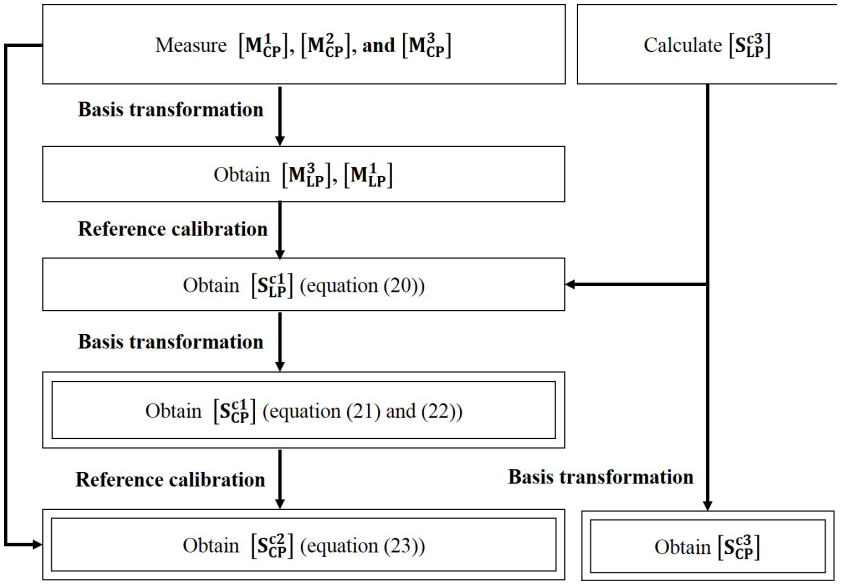

Figure 1. Flow diagram of the single reference calibration technique adopted in the CT1_CP.

Eq. (5) as

$$S_{LL}^{c1} = \frac{1}{2}\left(S_{HH}^{c1} - S_{VV}^{c1}\right), \tag{21}$$

$$S_{RR}^{c1} = \frac{1}{2}\left(S_{VV}^{c1} - S_{HH}^{c1}\right). \tag{22}$$

Note that S_{LR}^{c1} and S_{RL}^{c1} are theoretically zero (see Eq. (6a)). Therefore, the problem in obtaining the correct scattering matrix of a complex target can be still avoided for CP measurements by this way. The correct scattering matrix of the second calibration target, namely a dihedral 45° is easily obtained afterwards via (see Fig. 1)

$$\begin{bmatrix} S_{LL}^{c2} \\ S_{RR}^{c2} \end{bmatrix} = \begin{bmatrix} \dfrac{S_{LL}^{c1}}{M_{LL}^{3}} & 0 \\ 0 & \dfrac{S_{RR}^{c1}}{M_{RR}^{3}} \end{bmatrix} \begin{bmatrix} M_{LL}^{2} \\ M_{RR}^{2} \end{bmatrix}. \tag{23}$$

It is also worth to note that precise alignment of the calibration targets is needed to avoid errors between the calculated and the actual values of the backscattering coefficients. Although, this target orientation problem can be mostly resolved when operating in a GB laboratory conditions, it becomes significant when calibrating the radars mounted on a moving platform.

2.2. CT2_CP Calibration Process

The original LP based CT2 [23] assumes that the receiver distortion matrix [**R**] is the transpose of those transmitter's [**T**]. This assumption results in the six unknown error coefficients which are determined by means of only two calibration targets; a vertical dihedral for co-polarization and either 22.5° or 45° inclined dihedral for cross-polarization. Therefore, unlike the CT1, the CT2 assumes the distortion matrices of the radar error model, and thus it makes possible to reduce the number of the calibration targets.

For the adaptation of this technique to CP-basis, a vertical dihedral and a circular plate are selected as the co- and cross-polarized calibration targets, respectively (see Eqs. (6a) and (6c)). The formulation of the resulted CT2_CP is explained in the following.

The relationship between [**M**] and [$\mathbf{S^c}$] can be modeled as:

$$\begin{bmatrix} M_{LL}A_{LL} & M_{LR}A_{LR} \\ M_{RL}A_{RL} & M_{RR}A_{RR} \end{bmatrix} = \begin{bmatrix} 1 & \delta_y \\ \delta_x & 1 \end{bmatrix} \begin{bmatrix} S_{LL}^{c} & S_{LR}^{c} \\ S_{RL}^{c} & S_{RR}^{c} \end{bmatrix} \begin{bmatrix} 1 & \delta_x \\ \delta_y & 1 \end{bmatrix}, \tag{24}$$

where A is for the frequency response of each measured polarimetric channel, and δ is the crosstalk which means undesired polarized signals. If we denote a vertical dihedral as the [$\mathbf{S^{c1}}$] and a circular plate as the [$\mathbf{S^{c2}}$], these unknown parameters can be solved from the following equations with the assumption that $\delta_x \cdot \delta_y = 0$:

$$A_{LL} = \frac{S_{LL}^{c1}}{M_{LL}^{1}}, \tag{25}$$

$$A_{RR} = \frac{S_{RR}^{c1}}{M_{RR}^{1}}, \tag{26}$$

$$\delta_{\mathrm{y}} = \frac{A_{LL}M_{LL}^{2} - S_{LL}^{c2}}{2S_{LR}^{c2}}, \tag{27}$$

$$\delta_x = \frac{A_{RR}M_{RR}^{2} - S_{RR}^{c2}}{2S_{LR}^{c2}}, \tag{28}$$

$$A_{LR} = \frac{\delta_x S_{LL}^{c2} + S_{LR}^{c2} + \delta_y S_{RR}^{c2}}{M_{LR}^{1}}, \tag{29}$$

$$A_{RL} = \frac{\delta_x S_{LL}^{c2} + S_{RL}^{c2} + \delta_y S_{RR}^{c2}}{M_{RL}^{1}}. \tag{30}$$

Finally, calibrated scattering matrix $[\mathbf{S^c}]$ can be derived by

$$\begin{bmatrix} S^c_{LL} & S^c_{LR} \\ S^c_{RL} & S^c_{RR} \end{bmatrix} = \begin{bmatrix} 1 & \delta_y \\ \delta_x & 1 \end{bmatrix}^{-1} \begin{bmatrix} M_{LL}A_{LL} & M_{LR}A_{LR} \\ M_{RL}A_{RL} & M_{RR}A_{RR} \end{bmatrix} \begin{bmatrix} 1 & \delta_x \\ \delta_y & 1 \end{bmatrix}^{-1}. \tag{31}$$

S^{c1}_{LL} and S^{c1}_{RR} are derived from a circular plate as a reference target in the same manner as the single reference method explained in Subsection 2.1 (see Fig. 1).

Unlike its LP version, the CT2_CP does not need to employ an inclined dihedral as a calibration target. As noted in Subsection 2.1, the techniques that are sensitive to the target orientation might lead to significant errors in the calibration process. Therefore, this attribute of the CT2_CP can be regarded as an important advantage especially for the calibration of radars under field conditions.

3. EXPERIMENTAL RESULT

The validity of the CT1_CP and CT2_CP was evaluated through the GB frequency domain measurements. Both the scatterometric and SAR experiment in CP-basis were conducted within an anechoic chamber. In the scatterometric mode, the backscattering responses of the calibration targets, as well as test targets, were measured at only one view angle. In the SAR imaging mode, stripmap SAR data of a test target (i.e., vertical wire) were acquired along a 2.2 m long aperture. The SAR images were constructed by the ω-k SAR imaging algorithm [33].

In all measurements described below, a VNA (Agilent E8364C) operated in stepped-frequency mode was used, and the collected frequency domain data are empty room subtracted and range-gated.

3.1. Results for the Scatterometric Mode

The measurement geometry of this mode is depicted in Fig. 2. The elevation and azimuth angles were set to 0°, and only one static measurement within the frequency range of 4.5–7.5 GHz was performed with 801 sampling points. The antenna system consisted of two dual-polarized LP horn antennas in quasi-monostatic configuration. CP was achieved by a phase shifter between H and V channels. The distance from midpoint of antenna phase center to the target center was adjusted to 5.5 m that leads to a far-field illumination of targets.

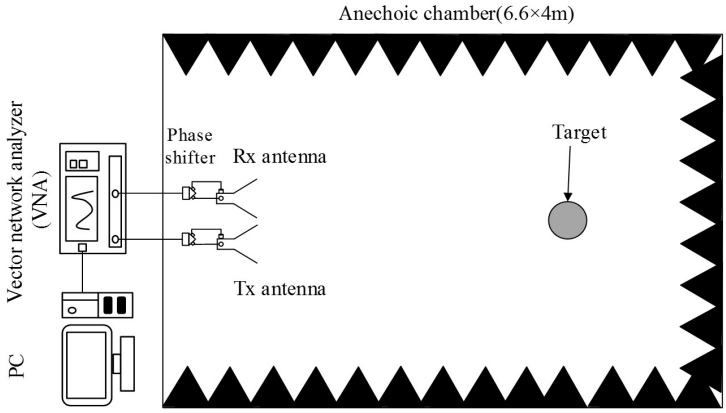

Figure 2. Experimental setup of the scatterometric measurement inside the anechoic chamber.

Table 1 shows the calibration and the test targets used in this experiment. As can be seen from Eqs. (6a) and (6c), a circular plate produces dominant scattering for cross-polarization whereas a dihedral produces strong reflection for co-polarization. Therefore, a circular plate and a dihedral were chosen as the test targets to calibrate cross-polarization (LR and RL) and co-polarization (LL and RR) data, respectively. The procedure adopted in the calibration of the scatterometric measurements is explained as follows:

Table 1. Calibration target and test targets used in the CT1_CP and the CT2_CP.

Targets	CT1_CP	CT2_CP
Cal target 1	Dihedral 45°	Vertical dihedral
Cal target 2	Vertical dihedral	Circular plate
Cal target 3	Circular plate	None
Test target 1	Circular plate	
Test target 2	Vertical dihedral	

(i) Measure the isolation matrix [**I**].
(ii) Measure the scattering matrices [$\mathbf{S^m}$] of all calibration targets and the test targets (Equation (1)).
(iii) Obtain empty room calibrated data [**M**] by subtracting [**I**] from the [$\mathbf{S^m}$] (Equation (2)).
(iv) Calculate the error coefficients of the two techniques by the measured [**M**] and the correct scattering matrices [$\mathbf{S^{ci}}$] of the calibration targets (Equations (11)–(18) and (25)–(30).
(v) Apply a correction to the measured scattering matrix of the test target (i.e., solve Equations (19) and (31) for the [$\mathbf{S^c}$] of the test target).
(vi) Compare the uncalibrated [**M**] and the calibrated [$\mathbf{S^c}$] scattering matrices in the frequency domain.

Firstly, the effectiveness of the cross-polarization calibration was evaluated by employing a circular plate test target with a diameter of 15 cm. The calibration targets were dihedral and circular plate as listed in Table 1 and with dimensions of $18 \times 18 \times 30$ cm and 30 cm diameter, respectively. The amplitude and phase imbalances between the channels are given in Figs. 3(a) and (b), respectively

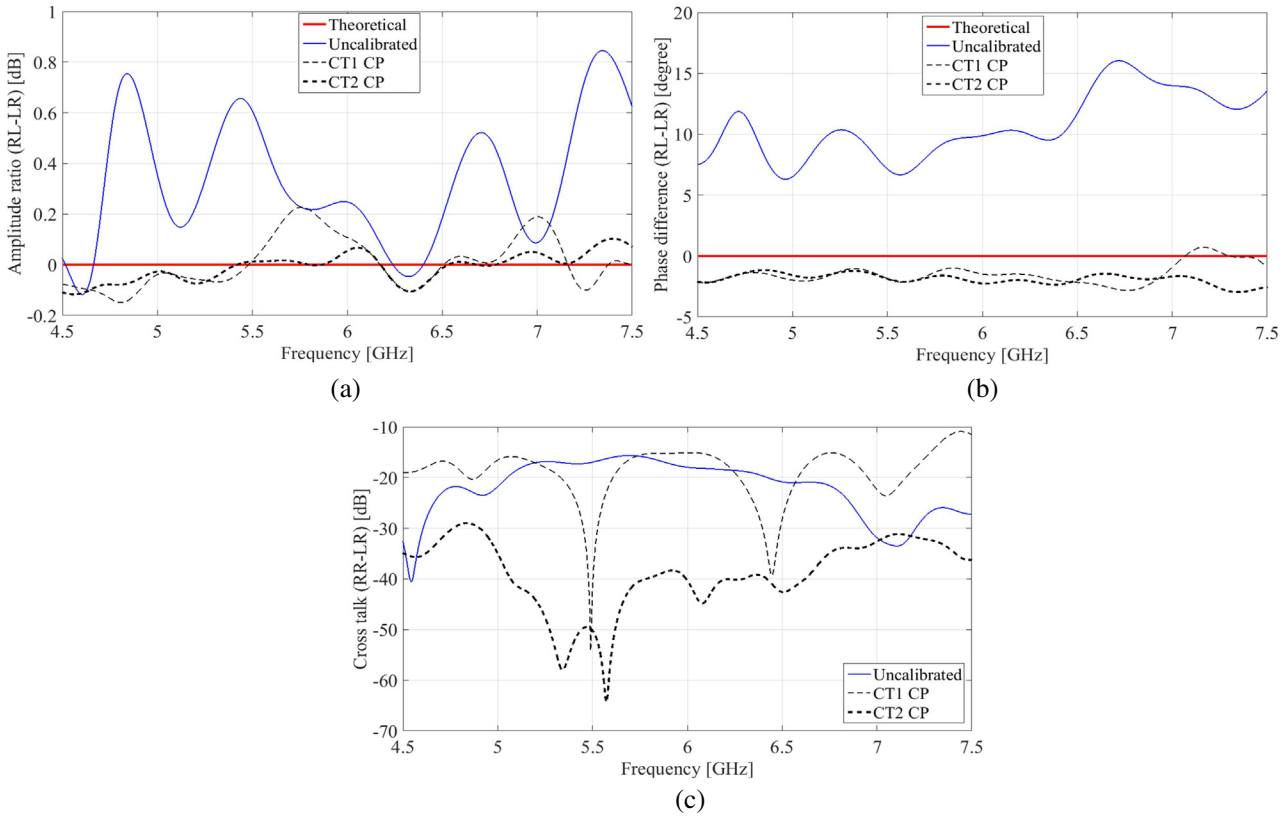

Figure 3. Cross-polarization calibration result of the circular plate test target: (a) Cross-polarization amplitude ratio (*RL-LR*), (b) cross-polarization phase difference (*RL-LR*), (c) crosstalk (*RR-LR*).

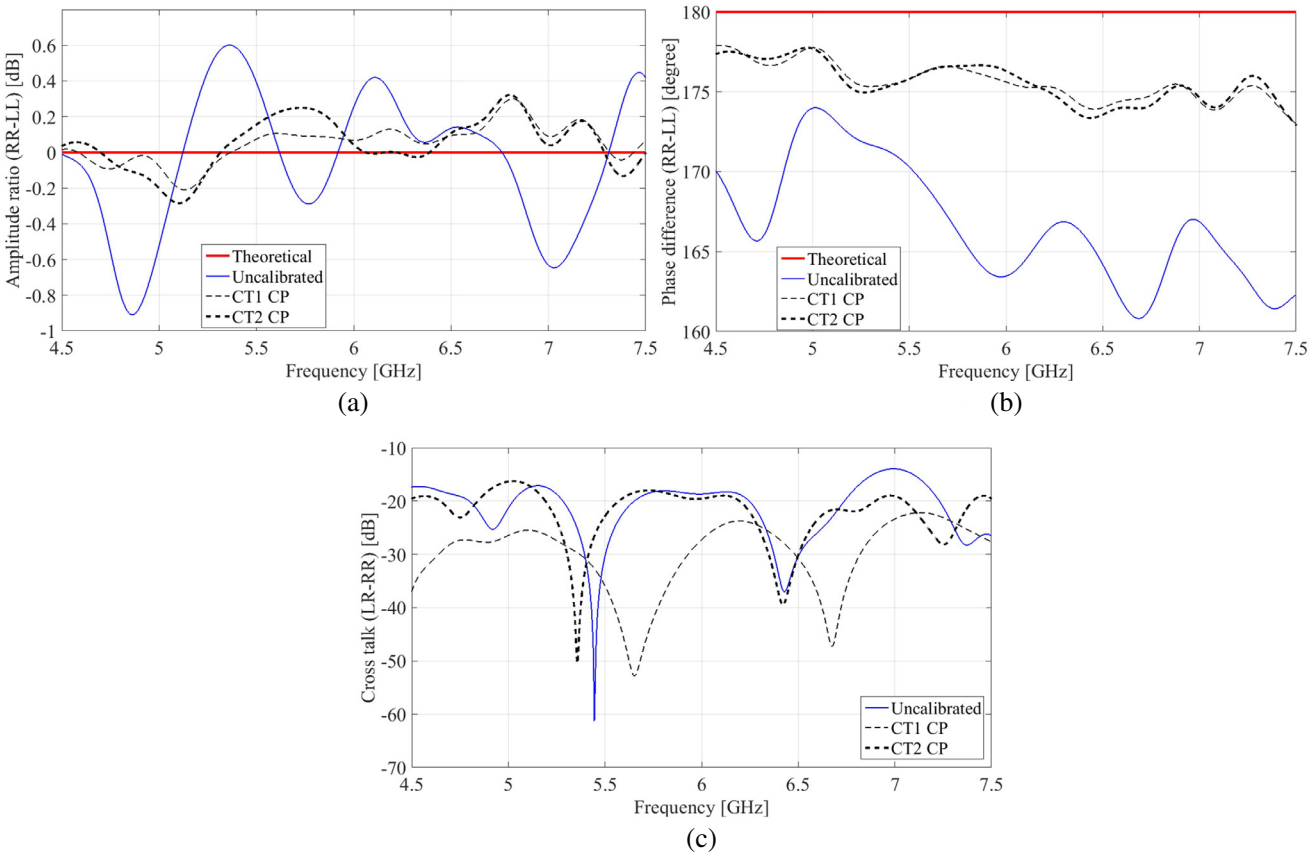

Figure 4. Co-polarization calibration result of the dihedral test target: (a) Co-polarization amplitude ratio (*RR-LL*), (b) co-polarization phase difference (*RR-LL*), (c) crosstalk (*LR-RR*).

which demonstrate that the phase difference (*RL-LR*) is improved from approximately 6° to $\sim 2°$ and the amplitude ratio (*RL-LR* in logarithmic scale) falls in the range of $\sim \pm 0.2$ dB after the calibration. The crosstalk calibration results (*RR-LR* in logarithmic scale) are illustrated in Fig. 3(c) which show a significant difference between CT1_CP and CT2_CP. From these figures, the result of the CT2_CP yields the reduction of ~ 20 dB, compared to uncalibrated value. However, the result of the CT1_CP does not provide any improved crosstalk result.

The co-polarization calibration performance was investigated by an $18 \times 18 \times 30$ cm vertical dihedral as a test target. The calibration targets for this case were a dihedral with $18 \times 18 \times 40$ cm dimension and a circular plate with 20 cm diameter. From the results given in Fig. 4, the calibrated amplitude ratio (*RR-LL*) is identified to be around ± 0.3 dB and the phase difference (*RR-LL*) shows $\sim 5°$ error after the calibration (Figs. 4(a) and (b)). The crosstalk result shown in Fig. 4(c) demonstrates reduction of ~ 10 to 30 dB for the CT1_CP and partial reduction of ~ 5 dB for the CT2_CP.

3.2. Results for the SAR Imaging Mode

The aim of this experiment is to test the performances of the CT1_CP and the CT2_CP for a more practical imaging and a polarimetric application. The polarimetric GB-SAR system constructed by a VNA, CP-antennas, a positioner controller, a positioner, and a PC is shown in Fig. 5. To reconstruct the SAR images, the ω-k algorithm was used [33]. An automatic position controller moved the target under test along a 2.2 meter long rail with 22 mm azimuth steps. Frequency range was again set to 4.5–7.5 GHz with 801 sampling points. An $18 \times 18 \times 30$ cm dihedral and a 30 cm diameter of a circular plate were used as the calibration targets and a vertical wire with 2 mm diameter was used as the test target. In this experiment, the calibration targets were measured only for the center position of this aperture.

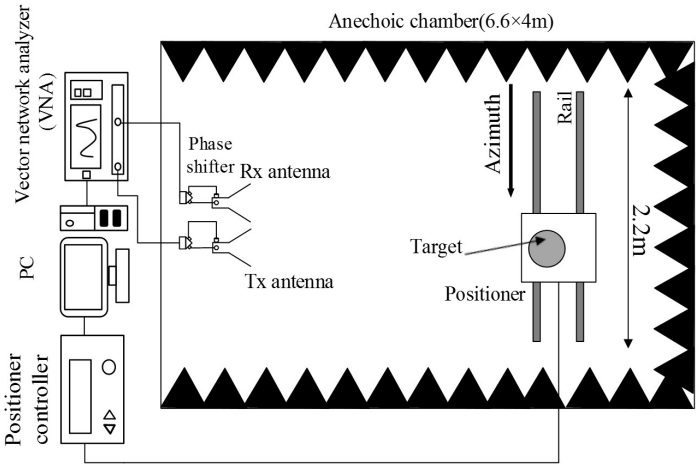

Figure 5. Experimental setup of the GB-SAR measurement inside the anechoic chamber.

Hence, neglecting the azimuth angle dependency, the error correction matrices were calculated only for this position and applied to all other azimuth data of the test target. The vertical wire was selected because the theoretical scattering matrix coefficients (LL, LR, RL, and RR) have the same absolute intensity value, shown as

$$\left[\mathbf{S}_{CP}^{\text{vertical wire}}\right] = \frac{C}{2}\begin{bmatrix} -1 & j \\ j & 1 \end{bmatrix}. \tag{32}$$

This factor can lead to an assessment of all polarizations. The quality of calibration was inferred from the SAR images by picking up and evaluating the scattering matrices at the target location. Moreover, the Cloude-Pottier eigenvector-based decomposition [34] was applied to the reconstructed SAR images (LL, LR, RL, and RR) to see the effect of calibration on target parameter retrievals such as radar a line of sight orientation and scattering mechanism. The procedure followed for calibrating SAR imagery is explained below:

(i) Calculate the error coefficients of the two techniques in the same manner to calibration procedure (i)–(iv) of scatterometric mode.

(ii) Collect SAR data of the test target.

(iii) Apply a correction to the test target's data measured at each azimuth position.

(iv) Reconstruct the SAR images of LL, LR, RL, and RR polarizations.

(v) Pick up the scattering matrices belonging to the target.

(vi) Compare these calibrated matrices with uncalibrated ones.

(vii) Apply the Cloude-Pottier eigenvector-based decomposition to the reconstructed SAR images (LL, LR, RL, and RR) of the target location.

The results for vertical wire of LL polarization are shown in Fig. 6, which are displayed on a normalized 40 dB dynamic range. It is worth noting that the effect of calibration usually cannot be observed from image data, and should be obtained by analysis of scattering matrices extracted from the target location and polarimetric decomposition which are explained in the following.

First, the scattering matrices of the target location (the pixel that has maximum value) are extracted with normalization to a maximum value of polarization channels. The obtained results given below represent the uncalibrated and the calibrated scattering matrices, respectively.

Scattering matrix extracted from the uncalibrated images:

$$[\mathbf{S}_{\text{uncalibrated}}] = \begin{bmatrix} 1.0000e^{j0^\circ} & 0.7291e^{j82.4328^\circ} \\ 0.7720e^{j88.9549^\circ} & 0.7941e^{j-175.5934^\circ} \end{bmatrix},$$

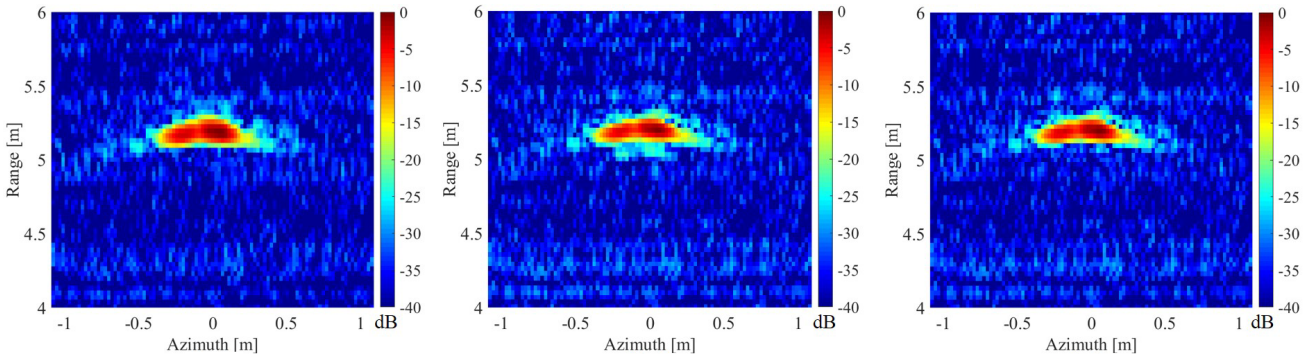

Figure 6. Vertical wire imaging results. (a) Uncalibrated LL image, (b) calibrated LL image applied by CT1_CP, (c) calibrated LL image applied by CT2_CP.

Table 2. Absolute amplitude ratio and relative phase difference of LL-LR and LL-RR of the vertical wire imaging result.

	Absolute amplitude ratio1 (LL-LR) [dB]	Absolute amplitude ratio2 (LL-RR) [dB]	Relative phase difference1 (LL-LR) [°]	Relative phase difference2 (LL-RR) [°]
Theoretical values	0	0	90	180
Uncalibrated values	2.7443	2.0025	82.4328	175.5934
CT1_CP	0.4047	0.2960	79.1009	172.3562
CT2_CP	0.2828	0.0087	82.7009	176.4070

Scattering matrix extracted from the CT1_CP calibrated images:

$$[\mathbf{S}_{\mathbf{CT1\_CP}}] = \begin{bmatrix} 0.9665e^{j172.3562^\circ} & 0.9225e^{j93.2553^\circ} \\ 0.9762e^{j97.1914^\circ} & 1.0000e^{j0^\circ} \end{bmatrix},$$

Scattering matrix extracted from the CT2_CP calibrated images:

$$[\mathbf{S}_{\mathrm{CT\_CP}}] = \begin{bmatrix} 0.9990e^{j176.4070^\circ} & 0.9670e^{j93.7061^\circ} \\ 0.9879e^{j98.4779^\circ} & 1.0000e^{j0^\circ} \end{bmatrix}.$$

To assess the obtained scattering matrices, the absolute logarithmic amplitude ratio and the relative phase difference of LL-LR and LL-RR are listed in Table 2. Both the calibrated amplitude imbalance results of the CT1_CP and CT2_CP show improvement of ~ 2.4 dB for the LL-LR and ~ 1.9 dB for the LL-RR compared to the corresponding uncalibrated measured values. In the case of the phase difference, the CT2_CP provides a small improvement (less than 1°) in both the LL-LR and the LL-RR. However, the CT1_CP degrades the result.

The polarimetric performances are then assessed by applying the Cloude-Pottier eigenvector-based decomposition that produces the scattering randomness and the physical parameters of the target of interest [34]. The entropy H, alpha angle $\bar{\alpha}$, and beta angle $\bar{\beta}$ were calculated for the target region. H accounts for the scattering randomness; $\bar{\alpha}$ represents an intrinsic scattering type (0° for surface scattering, 45° for wire scattering, and 90° for double-bounce and helix scattering); $\bar{\beta}$ is related to orientation angle about radar line of sight [34].

The uncalibrated and calibrated H-$\bar{\alpha}$ distributions are displayed in Fig. 7. Since our target is regarded as the point-target vertical wire, the distribution must be inside the zone 8 (Z8) of Fig. 7 which indicates the low entropy wire scattering [34]. However, some plots exhibit zone 7 (Z7) which

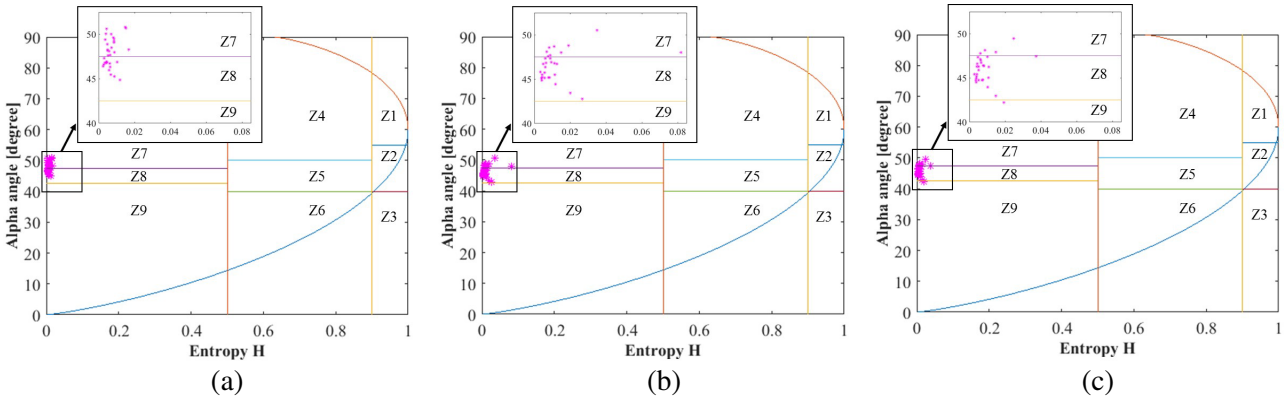

Figure 7. H-$\bar{\alpha}$ distribution from the target location of the CP-SAR images. (a) Uncalibrated data, (b) calibrated data applied by the CT1_CP, (c) calibrated data applied by the CT2_CP.

Table 3. H-$\bar{\alpha}$ distribution accuracy rate of Z8 and averaged $\bar{\beta}$ from the target location of the CP-SAR images.

	H-$\bar{\alpha}$ accuracy rate of Z8 [%]	Averaged $\bar{\beta}$ [°]
Theoretical values	100.0	0
Uncalibrated values	43.3	9.0118
CT 1_CP	66.7	6.6481
CT2_CP	86.2	4.4254

shows low entropy double bounce scattering such as the point-target dihedral. Therefore, the accuracies of the H-$\bar{\alpha}$ distributions which are the rate of plots inside of the Z8 are calculated and listed in Table 3. From Table 3, both the CT1_CP and CT2_CP yield an increase of the accuracy rate relative to the uncalibrated value.

The calculated beta angles are averaged over the target regions. Theoretically, $\bar{\beta}$ has a value of 0° for the vertical wire target. In Table 3, the theoretical, uncalibrated, and calibrated averaged beta angles are listed. The results calibrated by both the CT1_CP and the CT2_CP exhibit 6.6481° and 4.4254° respectively which are closer value to the theoretical 0° than the uncalibrated one.

4. DISCUSSION

Compared to the existing CP-calibration method developed by Michelson et al. [28] wherein a complex depolarizing trihedral is used, the proposed techniques utilize only canonical calibration targets (i.e., circular plate and dihedral). Moreover, both proposed methods in this paper cover the single reference calibration technique, where only the knowledge of theoretical scattering matrix of a circular plate is required to determine all the correct scattering matrix of calibration targets. This factor leads to the accurate calibration performance. Non-usage of an inclined reflector in the CT2_CP can also be regarded as an important benefit over the LP-basis techniques, which often require either inclined or complex structured targets to achieve the cross-polarization calibration. When compared to each other (the CT1_CP and the CT2_CP), the CT2_CP requires less number of calibration targets with easier alignment than the CT1_CP.

The scatterometric experiment results reveal that the calibration methods yield similar and effective performance for the amplitude and the phase imbalances across the investigated frequency bandwidth. However, the crosstalk results exhibit strong dependency on the calibration method. The crosstalk results of the CT1_CP for cross-polarization and the CT2_CP for co-polarization were not improved effectively in this experiment. This problem might be mitigated under more precise measurement to suppress the depolarization effect. This needs further investigation.

The SAR imaging experiment demonstrated well calibrated results for the amplitude ratio and the Cloude-Pottier eigenvector-based decomposition parameters when the vertical wire was selected as a test target. However, improvements of the phase difference were seen only in the CT2_CP not in the CT1_CP. From the series of assessment for the SAR imaging experiment, the CT2_CP yielded better calibration capability than the CT1_CP over the channel imbalance of single scattering matrix, the accuracy rate of H-$\bar{\alpha}$ distribution, and the $\bar{\beta}$.

5. CONCLUSION

Two point target-based polarimetric calibration techniques for the GB CP-radar were investigated. The techniques were experimentally validated and compared through scatterometric and SAR imaging experiments for the wide frequency bandwidth in C-band. In the scatterometric experiment, the calibration performances were confirmed on cross-polarization and co-polarization by a circular plate and a vertical dihedral as the test targets, respectively. This measurement resulted in a satisfactory channel imbalances and reduction of crosstalk. The crosstalk calibration results exhibited reduction in either the CT1_CP or the CT2_CP. In the SAR imaging experiment, the calibration performances were evaluated by considering the channel imbalances of scattering matrices and the Cloude-Pottier eigenvector-based decomposition. Both techniques improved the amplitude imbalance of scattering matrix, the accuracy rate of H-$\bar{\alpha}$ distribution, and the $\bar{\beta}$ for the vertical wire. The phase imbalance improvements on the CT2_CP were also confirmed, however, the CT1_CP degraded.

Overall, the results illustrate that each calibration technique shows satisfactorily good performance. However, the proposed techniques still showed minor unstable results. Therefore, further study of the point target-based CP calibration is anticipated for different calibration target sets and procedures.

This GB study is a step towards developing polarimetric calibration technique for a CP-radar onboard UAV, aircraft, and satellite.

ACKNOWLEDGMENT

This work was supported in part by the European Space Agency Earth Observation Category 1 under Grant 6613, by the 4th Japan Aerospace Exploration Agency (JAXA) ALOS Research Announcement under Grant 1024, by the 6th JAXA ALOS Research Announcement under Grant 3170, by the Japanese Government National Budget (Special Budget for Project) FY 2015 under Grant 2101, Taiwan National Space Organization under Grant NSPO-S-105096; Indonesian Bhimasena, and by the Chiba University Strategic Priority Research Promotion Program FY 2016.

REFERENCES

1. Moreira, A., P. Prats-Iraola, M. Younis, G. Krieger, I. Hajnsek, and K. P. Papathanassiou, "A tutorial on synthetic aperture radar," *IEEE Geoscience and Remote Sensing Magazine*, Vol. 1, No. 1, 6–43, 2013.
2. Henderson, F. M. and J. L. Anthony, *Principles and Applications of Imaging Radar*, John Wiley and Sons, NY, 1998.
3. Lee, J. S. and E. Pottier, *Polarimetric Radar Imaging from Basics to Applications*, CRC Press, FL, 2009.
4. Cloude, S., *Polarization: Applications in Remote Sensing*, Oxford University Press, 2010.
5. Zhou, Z. S., W. M. Boerner, and M. Sato, "Development of a ground-based polarimetric broadband SAR system for noninvasive ground-truth validation in vegetation monitoring," *IEEE Transactions on Geoscience and Remote Sensing*, Vol. 42, No. 9, 1803–1810, 2004.
6. Malz, E., R. Zetik, P. Semashko, R. S. Thoma, and A. G. Ariza, "Polarimetric ultrawideband radar," *2012 IEEE International Geoscience and Remote Sensing Symposium*, 5919–5922, Munich, 2012.

7. Zhou, Z. S. and S. Cloude, "Structural parameter estimation of Australian flora with a ground-based polarimetric radar interferometer," *2006 IEEE International Symposium on Geoscience and Remote Sensing*, 71–74, Denver, 2006.
8. Martorella, M., E. Giusti, A. Capria, F. Berizzi, and B. Bates, "Automatic target recognition by means of polarimetric ISAR images and neural networks," *IEEE Transactions on Geoscience and Remote Sensing*, Vol. 47, No. 11, 3786–3794, 2009.
9. Lopez-Sanchez, J. M., J. D. Ballester-Berman, V. D. Navarro-Sanchez, and F. Vicente-Guijalba, "Experimental validation of the interferometric coherence formulation in single-transmit mode," *2012 IEEE International Geoscience and Remote Sensing Symposium*, 3114–3117, Munich, 2012.
10. Salman, R., I. Willms, L. Reichardt, T. Zwick, W. Wiesbeck, and R. S. Thoma, "On buried weapon detection by means of scattering matrix decomposition for quad-polarized ultra-wideband radar," *2013 IEEE International Conference on Ultra-Wideband (ICUWB)*, 113–119, Sydney, 2013.
11. Gomez-Dans, J. L., S. Quegan, and J. C. Bennett, "Indoor C-band polarimetric interferometry observations of a mature wheat canopy," *IEEE Transactions on Geoscience and Remote Sensing*, Vol. 44, No. 4, 768–777, 2006.
12. Sri-Sumantyo, J. T., V. C. Koo, T. S. Lim, T. Kawai, T. Ebinuma, Y. Izumi, M. Z. Baharuddin, S. Gao, and K. Ito, "Development of circularly polarized synthetic aperture radar on-board UAV JX-1," *International Journal of Remote Sensing*, 1–12, 2017.
13. Rizki Akbar, P., J. T. Sri-Sumantyo, and H. Kuze, "A novel circularly polarized synthetic aperture radar (CP-SAR) system onboard a spaceborne platform," *International Journal of Remote Sensing*, Vol. 31, No. 4, 1053–1060, 2010.
14. Izumi, Y., S. Demirci, M. Z. Baharuddin, J. T. Sri Sumantyo, and H. Yang, "Analysis of circular polarization backscattering and target decomposition using GB-SAR," *Progress In Electromagnetics Research B*, Vol. 73, 17–29, 2017.
15. Freeman, A., "Calibration of linearly polarized polarimetric SAR data subject to Faraday rotation," *IEEE Transactions on Geoscience and Remote Sensing*, Vol. 42, No. 8, 1617–1624, 2004.
16. Goh, A. S., "Bistatic synthetic aperture radar data processing and analysis," Doctoral dissertation, The University of Adelaide, 2012.
17. Van-Zyl, J. J., "Calibration of polarimetric radar images using only image parameters and trihedral corner reflector responses," *IEEE Transactions on Geoscience and Remote Sensing*, Vol. 28, No. 3, 337–348, 1990.
18. Quegan, S., "A unified algorithm for phase and cross-talk calibration of polarimetric data-theory and observations," *IEEE Transactions on Geoscience and Remote Sensing*, Vol. 32, No. 1, 89–99, 1994.
19. Ainsworth, T. L. and J. S. Lee, "A new method for a posteriori polarimetric SAR calibration," *2001 IEEE International Geoscience and Remote Sensing Symposium — IGARSS*, 420–422, Sydney, 2001.
20. Freeman, A., "SAR calibration: An overview," *IEEE Transactions on Geoscience and Remote Sensing*, Vol. 30, No. 6, 1107–1121, 1992.
21. Yueh, S. H., J. A. Kong, and R. T. Shin, "Calibration of polarimetric radars using in-scene reflectors," *Progress In Electromagnetics Research*, Vol. 3, 451–510, 1990.
22. Sarabandi, K., F. T. Ulaby, and M. A. Tassoudji, "Calibration of polarimetric radar systems with good polarization isolation," *IEEE Transactions on Geoscience and Remote Sensing*, Vol. 28, No. 1, 70–75, 1990.
23. Gau, J. R. and W. D. Burnside, "New polarimetric calibration technique using a single calibration dihedral," *IEE Proceedings — Microwaves, Antennas and Propagation*, Vol. 142, No. 1, 19–25, 1995.
24. Whitt, M. W., F. T. Ulaby, P. Polatin, and V. V. Liepa, "A general polarimetric radar calibration technique," *IEEE Transactions on Antennas and Propagation*, Vol. 39, No. 1, 62–67, 1991.
25. Chen, T. J., T. H. Chu, and F. C. Chen, "A new calibration algorithm of wide-band polarimetric measurement system," *IEEE Transactions on Antennas and Propagation*, Vol. 39, No. 8, 1188–

1192, 1991.

26. Wiesbeck, W. and D. Kahny, "Single reference, three target calibration and error correction for monostatic, polarimetric free space measurements," *Proceedings of the IEEE*, Vol. 79, No. 10, 1551–1558, 1991.
27. Wiesbeck, W. and S. Riegger, "A complete error model for free space polarimetric measurements," *IEEE Transactions on Antennas and Propagation*, Vol. 39, No. 8, 1105–1111, 1991.
28. Michelson, D. G., I. G. Cumming, and C. E. Livingstone, "A calibration algorithm for circular polarimetric radars," *Journal of Electromagnetic Waves and Applications*, Vol. 11, No. 5, 659–674, 1997.
29. Michelson, D. G. and E. V. Jull, "Depolarizing trihedral corner reflectors for radar navigation and remote sensing," *IEEE Transactions on Antennas and Propagation*, Vol. 43, No. 5, 513–518, 1995.
30. Sheen, D. R., E. L. Johansen, L. P. Elenbogen, and E. S. Kasischke, "The gridded trihedral: A new polarimetric SAR calibration reflector," *IEEE Transactions on Geoscience and Remote Sensing*, Vol. 30, No. 6, 1149–1153, 1992.
31. Ruck, G. T., *Radar Cross Section Handbook*, Plenum Press, New York, 1970.
32. Izumi, Y., S. Demirci, M. Z. Baharuddin, and J. T. Sri-Sumantyo, "The polarimetric calibration method for ground-based circularly polarized synthetic aperture radar," *PIERS Proceedings*, 5131–5135, Shanghai, China, Aug. 8–11, 2016.
33. Soumekh, M., *Synthetic Aperture Radar Signal Processing*, John Wiley and Sons, New York, 1999.
34. Cloude, S. R. and E. Pottier, "An entropy based classification scheme for land applications of polarimetric SAR," *IEEE Transactions on Geoscience and Remote Sensing*, Vol. 35, No. 1, 68–78, 1997.